Green Chemistry

Growth Kinetics of Humins Studied via X-Ray Scattering

Journal:	*Green Chemistry*
Manuscript ID	GC-ART-11-2019-003961.R1
Article Type:	Paper
Date Submitted by the Author:	19-Feb-2020
Complete List of Authors:	Cheng, Ziwei; University of Delaware, Chemical Engineering Goulas, K.; Oregon State University, CBEE Rodriguez Quiroz, Natalia; University of Delaware, Chemical Engineering Saha, Basudeb; University of Delaware, Catalysis Center for Energy Innovation; Vlachos, Dion; Univ. of Delaware,

Growth Kinetics of Humins Studied via X-Ray Scattering

Ziwei Cheng[1,2], Konstantinos A. Goulas [2, §], Natalia Quiroz Rodriguez[1,2], Basudeb Saha[2,*], and Dionisios G. Vlachos[1,2,*]

[1]Department of Chemical and Biomolecular Engineering

[2]Catalysis Center for Energy Innovation

University of Delaware, Newark, DE 19716, USA

§ Present address: Oregon State University, School of Chemical, Biological and Environmental Engineering, 105 SW 26th Street, 116 Johnson Hall, Corvallis, OR 97331

Abstract

We use ultra-Small Angle X-ray Scattering (USAXS) to investigate the evolution of size, morphology, volume fraction and number concentration of humins formed during dehydration of fructose to 5-hydroxymethylfurfural (HMF), and the further polymerization of HMF between 80-95 °C in 1 M hydrochloric acidic solutions. The radius of gyration (R_g) of suspended humins particles grows linearly with time and is accompanied by an increase in polydispersity (PD), before possible precipitation occurs. The scattering patterns indicate fractal-like structures. The apparent activation energy of humins growth is 102±0.4 kJ/mol. The trends in the number of particles over time reveal competing processes entailing the continuous formation of new particles (nucleation) leading to increasing polydispersity with time and the aggregation of existing particles and possible precipitation. The direct observation of growth of humins indicates that humins form primarily from HMF rather than fructose.

Keywords: Humins, biomass, fructose, 5-hydroxymethylfurfural, X-ray scattering, kinetics, particle growth

Introduction

Humins are waste by-products formed during acid-catalyzed hydrothermal processing of sugars to platform molecules, such as 5-hydroxymethylfurfural (HMF),[1] from uncontrolled cross-polymerization reactions of HMF and reaction intermediates.[1] Their formation has a detrimental effect on process economics, as humins are of low-value products that can only be used for combustion[2] or syngas production[3, 4]. Additionally, they can cause reactor plugging and maintenance issues. Efforts to transform humins to value-added products[3, 5] are hindered by limited understanding of the mechanism of their formation. Although the chemical constituents of humins have been elucidated using infrared [6] (IR) and nuclear magnetic resonance (NMR) [1, 7, 8] spectroscopy, certain aspects of their structure remains poorly understood. First, the number and the types of C-C and C-O linkages have not been determined. Second, their microstructure has not been studied in detail. The formation and growth of humins were studied by Tsilomelekis et al.[6] using low temperature dynamic light scattering (DLS) of a 5 wt% aqueous HMF solution. At 70 ºC, pH of 1 and reaction times less than 3 h, the hydrodynamic radius (R_H) of humins particles grows at a constant rate of 2.4 nm/min.[6] Studies using the DLS instrument were limited to a maximum temperature of ~70 °C. At these temperatures, the conversion of fructose to HMF is too slow, and thus, studies of humins formation from fructose via DLS cannot practically be conducted. Furthermore, the particle size at longer reaction times could not be measured due to the increasing turbidity and light absorption by the sample. Both of these phenomena were associated with the precipitation of larger particles.

In order to overcome the above limitations of DLS, here we use *in-situ* ultra-small angle X-ray scattering (USAXS) to monitor the size and morphology of fructose-derived humins particles over time. Given the X-ray transparency of the samples, we reasoned that X-ray scattering would not be influenced by the turbidity or the color of the samples. First, we present the growth of humins from fructose, as a function of temperature and time. We then use fructose and HMF as two separate substrates to qualitatively differentiate the two competing pathways of nucleation and growth. Lastly, a refined humins formation and growth scheme is proposed.

Methods

Materials

D-fructose (≥99% purity, Sigma Aldrich), 5-hydroxymethylfurfural, and hydrochloric acid, (37 wt%, Fisher Scientific) were purchased from Sigma-Aldrich and used without further purification. The hydrochloric acid solutions were prepared by diluting a 37 wt% concentrated stock using deionized water.

Ultra-Small Angle X-ray Scattering

Small Angle X-ray Scattering (SAXS) is a well-established tool to obtain information about colloidal samples such as size, shape, volume fraction, and interactions between the scatterers.[9] A brief review of the basic principles of SAXS can be found in the Supplementary Information.

In-situ Ultra-Small Angle X-ray Scattering (USAXS) experiments for the growth of humins were conducted at the X-ray Science Division beamline 9-ID-C at the Advanced Photon Source, Argonne National Laboratory (ANL). It is a versatile instrument that provides a wide range of q values to probe length scales ranging from nanometers to microns. We used photons with X-ray wavelength of 0.59 Å, obtained by beamline monochromator equipped with Si (111) optics. This USAXS instrument uses Bonse-Hart geometry to reach ultra-small angles of q = 0.0001 $Å^{-1}$ and can be optionally combined with SAXS and wide-angle X-ray scattering (WAXS) pinhole devices to cover range all the way up to q =6 $Å^{-1}$. Details regarding this specific instrument can be found elsewhere.[9] For our experiments, however, only the USAXS setup, was used. The beam size was 0.8 × 0.8 mm. The USAXS instrument was operated in slit smeared configuration with slit length of 0.028 $Å^{-1}$.

In a typical experiment, 0.3 mL of aqueous solution of 10 wt% fructose acidified with HCl to a pH value of 0 was injected into an NMR tube (Fisher Scientific, Catalog No.16-800-161). The samples were heated in a 10-slot temperature-controlled aluminum capillary holder. A USAXS scan was taken every 3 minutes. For each scan, the fast scan mode was used, covering the q range of 1×10^{-4} to 0.3 $Å^{-1}$ in 90 s.

Data reduction and analysis were done with the Irena software package in IGOR Pro 7.01 using the procedure described by Ilavsky et al.[12] In brief, data was fitted in slit smeared form using the Irena data analysis package.[12] A unified fit model for dilute spheroids was used to obtain the power-law slope from the Porod regime.[13] A Gaussian size distribution model for dilute spheroids was used to obtain the mean R_g and the standard deviation. An example of the fit is shown in Figure S1. The volume fraction (φ) can also be given by the software. The total number of particles per volume of solution can be calculated from the volume fraction and the particle size.

Typical Reactivity Experiments

To determine the concentration of HMF as a function of time during humins growth, a typical time-dependent experiment was done in which a 5 mL glass vial was loaded with 2 mL of the reaction mixture. The composition of the reaction mixture was the same as that used for the USAXS experiment. Each vial was sealed with a crimp cap and put into an oil bath preheated at 80-95 °C depending on the specific experiment. To be consistent with the reaction conditions at the USAXS beamline at ANL, no stirring of the reaction mixture was used. After desired reaction times, each vial was taken out and immediately placed in an ice bath to quench the reaction.

Analysis of the Soluble Reaction Products

To determine the conversion of fructose and the yields of the HMF, levulinic acid (LA) and formic acid (FA), the filtrate was diluted tenfold and analyzed using high-performance liquid

chromatography (Waters 2695 HPLC) equipped with a refractive index detector (RID, Waters model 2414) and a separation column (Aminex HPX-87H). A 5 mM aqueous sulfuric acid solution was used as the mobile phase at a flow rate of 0.5 mL/min. The column compartment temperature was maintained at 50 °C and the refractive index detector temperature was 35 °C. The characteristic peaks for the products and reactants were identified from the retention times of the individual primary standards. Each peak was integrated, and the actual concentration of each product was calculated from their respective pre-calibrated plots of peak area vs. concentration.

Results and Discussion

To understand the structural evolution of the suspended humins particles, we recorded USAXS spectra during fructose dehydration at different temperatures. A representative raw scattered intensity I(q) vs. scattering vector (q) plot is given for one set of conditions at various times in Figure 1a. Figure 1b shows a zoom-in at 62 minutes of reaction time. The scattered intensity I(q) increases with time at low q values (0.0002-0.002 $Å^{-1}$) but remains low and slow varying at higher q values. As such, we analyze the data of the low q regime that provides quantitative information. The radius of gyration as a function of time and temperature is depicted in Figure 2. At short reaction times for all four temperatures, the scattering was too weak to extract meaningful particle size data. At intermediate times and lower temperatures (80 and 85 °C), the R_g increases linearly with time, while at longer times, the growth slows down. The same trend in particle size vs. time was also reported by Tsilomelekis et al. [6] The linear regime at short times indicates the lack of diffusion limitations (a square root dependence is common for diffusion-limited growth). We attribute the plateau in R_g to the precipitation of the large suspended humins particles (see also below). Apart from precipitation, the scattering pattern collected at longer times suggests the formation of a secondary, smaller size population (Figure 1b, between 0.001 and 0.01 $Å^{-1}$), whose intensity was too weak to be fitted. This small population indicates that new, small size humins form during most of the growth period. At higher temperatures (90 and 95 °C), R_g continuously increases before exceeding the detection limit of the USAXS instrument and therefore a plateau was not observed. In all cases, the power law slopes of the scattering patterns range between 3 and 4, indicating the suspended particles have fractal-like rough surfaces.[13] This finding is consistent with the rough spheres observed in prior work using SEM imaging of humins.[4, 6, 8] The lack of a plateau along with the larger R_g values at higher temperatures indicate that the particle size alone is not sufficient to demarcate the existence of a plateau and precipitation as the main physical phenomenon. The particle density at a given size and the growth vs. precipitation rates collectively affect the observed behavior. Figure 2 underscores that the growth of humins particles is controlled by multiple chemical and physical phenomena. In the linear regime (short times), where similar phenomena happen and comparison between data is straightforward, the growth rate has a clear, monotonic dependence on temperature, with higher temperature leading to faster growth. The change in slope for the lower temperature experiments indicates a change in behavior. Humins particles formed at lower temperatures (80 and 85 °C) appear denser and precipitate at longer times (upon change in

slope), whereas particles grown at higher temperatures are less dense and keep growing further until the instrument detection limit is reached. Comparison of particles should be done in the same growth regime, e.g., the linear one, to capture similar phenomena.

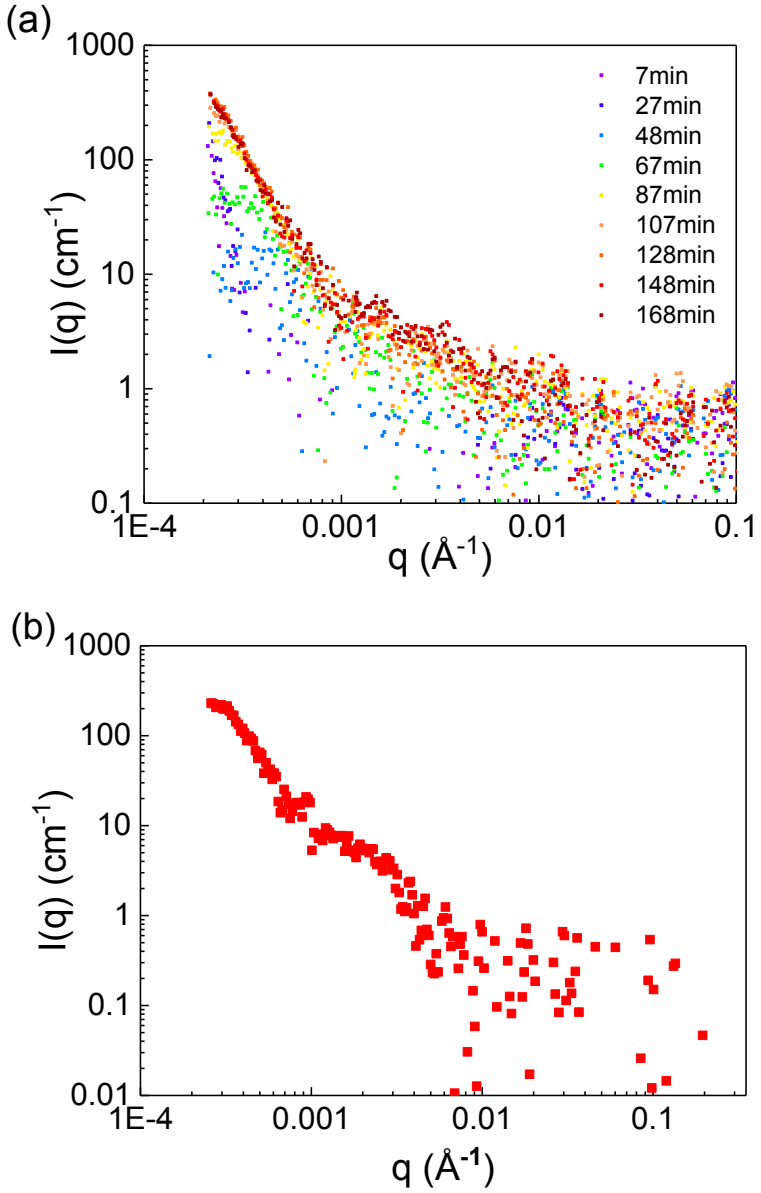

Figure 1. (a) Evolution of I(q) vs. q in a typical experiment. Data shown here were obtained from the reaction of 10 wt% fructose aqueous solution acidified with HCl to a pH of 0 and heated at 80 ºC. (b) I(q) vs. q plot at 62 min of reaction time for 10 wt% fructose at pH of 0 and 85 °C. The two Guinier-Porod regimes at 0.00026-0.001 $Å^{-1}$ and 0.001-0.01 $Å^{-1}$ indicate two particle size populations. Due to the weak intensity, scattering from the second population at higher q could not be fitted.

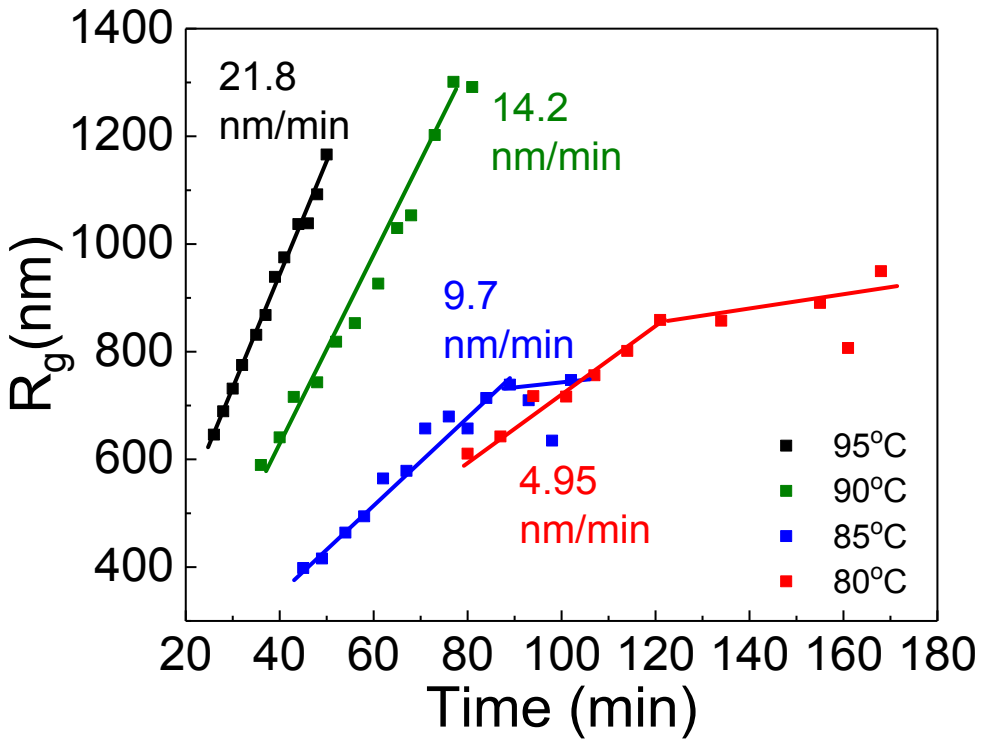

Figure 2. Mean radius of gyration (R_g) of humins particles as a function of time at various temperatures grown in a 10 wt% fructose solution at pH = 0. The lines guide the eye. Growth rates correspond to the initial growth regime (before the plateau when one is observed).

Taking the derivative dR_g/dt of the first regime (shorter times), we constructed an Arrhenius plot to obtain an apparent activation energy E_{app} for the humins formation (Figure 3) of 102±0.4 kJ/mol. It is worth noting that this value is determined by directly monitoring the growth rates of humins. The apparent activation energy inferred directly from the SAXS data captures not only chemistry but also physical adsorption and oligomer condensation. This is in contrast to the common literature method of determining the yields of fructose, FA and LA, and by estimating the amount of humins from the carbon balance. As a result, direct comparison of our $E_{a,\,app}$ with literature E_a values should be done with caution. In analogy to systems involving both diffusion and reaction, where the apparent activation energy is lower compared to the intrinsic activation energy, it is possible that the estimated value from the scattering experiments is a lower bound for chemical events.

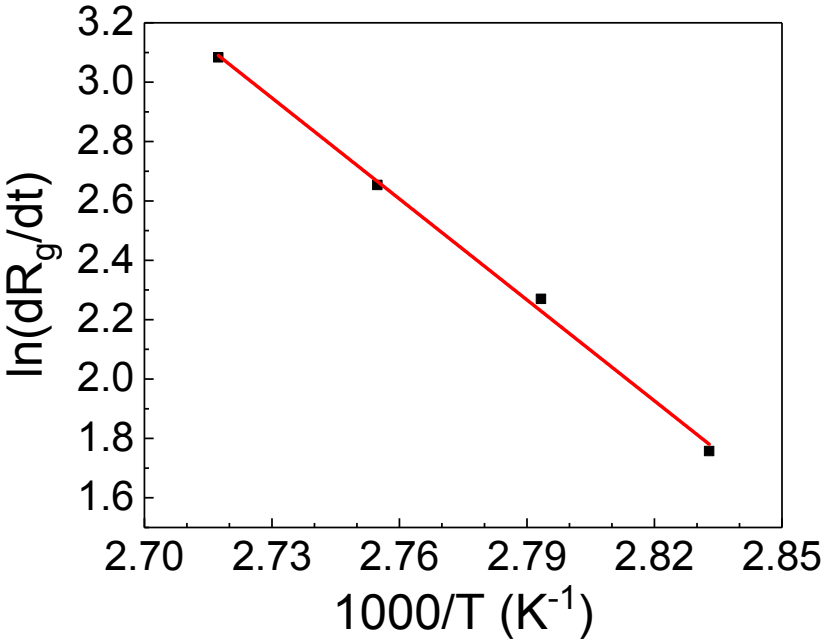

Figure 3. Arrhenius plot for humins formation rate from fructose at 80, 85, 90 and 95 ºC. A linear fit gives an R^2 value of 0.998 and an apparent activation energy E_{app} of 102±0.4 kJ/mol.

Figure 4 shows the change in the polydispersity index (PD) of humins particles over time. From 40 to 100 minutes of the reaction at 85 ºC, the PD of humins increases from 0.1 to as high as 0.6. The continuous formation of new particles was also been inferred in the work of Tsilomelekis et al.[6] using SEM to monitor the morphology of humins at different HMF conversions. The gradual increase in PD is consistent with the Carothers' equation,[16] suggesting that the humins follow a step-growth polymerization model that does not require an initiator. In this model, the monomers react with each other to form dimers, trimers, longer oligomers and eventually polymer networks. Continuous formation of humins, rather than an initial burst in nucleation, is consistent with the increasing polydispersity with time.

Next, we varied the initial fructose concentration and monitored the particle volume fraction and R_g. Figure 5a shows a much higher volume fraction of particles at higher fructose concentration. Yet, Figure 5b shows that the growth rate is independent of fructose concentration, and identical (within experimental error) to that when HMF is the substrate. These findings strongly suggest that fructose barely participates in humins formation. Combined with prior work, showing new IR peaks in humins when fructose is the reactant,[17] the results indicate adsorption of the sugar onto the humins rather than chemical incorporation. Interestingly, the number of particles per solution-volume increases over time for 50 wt % fructose but decreases for 10 wt % fructose (Figure 5c). The same dependence is also observed at other temperatures (at 85, 90 and 95 °C for 10 wt % fructose; Figure S2a, and at 70 and 80 °C for 50 wt % fructose; Figure S2b; see Supplementary Information (SI)). We attribute the larger number of particles at higher fructose concentrations to the higher HMF concentration that drives nucleation of new humins. The increase (decrease) of the population arises from competing mechanisms discussed below.

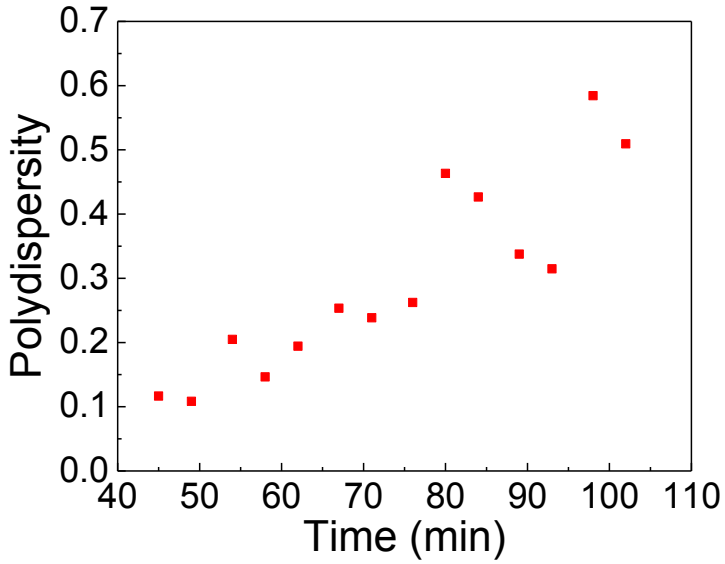

Figure 4. Evolution of polydispersity PD of growing humins over time at 85°C from a 10 wt% fructose solution at pH of 0. A Gaussian size distribution was used to obtain the mean and variance of particle sizes needed to calculate the PD.

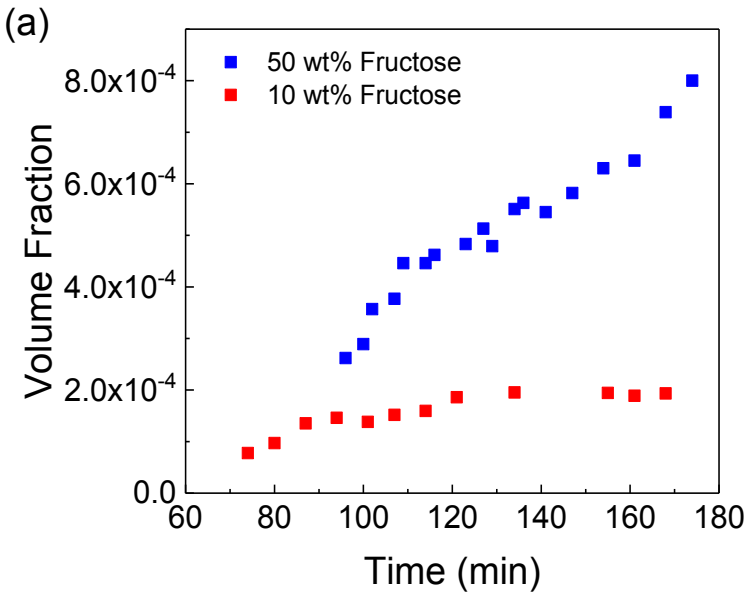

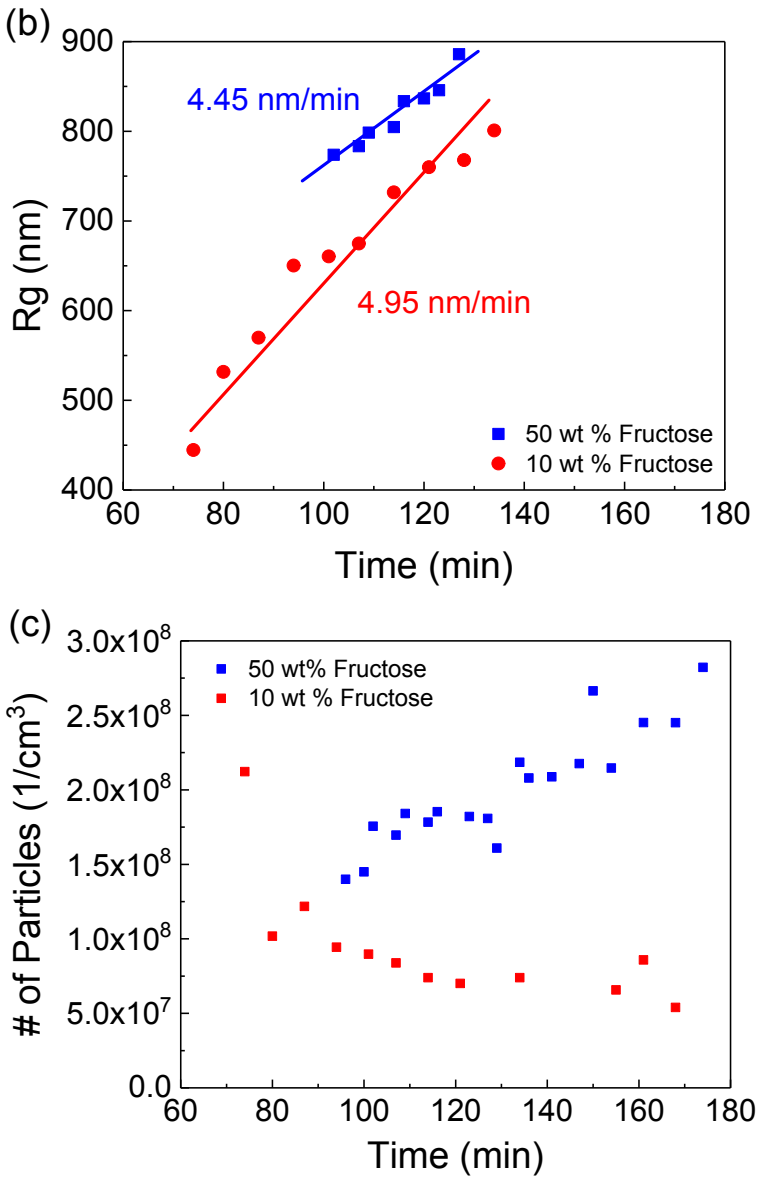

Figure 5. Evolution of (a) volume fraction of humins particles, (b) radius of gyration (R_g), and (c) number of particles per volume of solution at 50 wt% and 10 wt% initial fructose concentrations. Reaction at 80 °C and pH=0.

In most early kinetics studies,[18, 19] fructose was assumed to convert to an unknown intermediate which subsequently reacts with HMF to form humins. To our knowledge, the only Brønsted-catalyzed fructose dehydration kinetics study at low temperature (70-150 °C) which included the direct conversion of fructose to humins was published by Swift et al. [20] The reported reaction rate for the conversion of fructose to humins was faster than that of HMF to humins. The difference from our observations could be due to the literature model assumption that all five tautomers of fructose directly convert to humins at identical rates or model uncertainty arising from multiple sets of parameters in regression. Very little literature data is available for the

degradation of fructose tautomers in water other than β-pyranose, which only accounts for 45-55% of all the fructose over our temperature range as shown by Kimura et al.[21] and by Swift et al.[22] Swift et al. also used a KCl buffer in their experiments, which is known to decrease the selectivity to humins.[23] Although the effect of KCl on the kinetics of each pathway to humins has not been studied in detail, a recent *in-situ* Raman spectroscopy study by Ramesh et al.[24] showed that the molecular structures of glucose-derived humins formed in the presence of metal chloride catalysts $AlCl_3$ and $SnCl_4$ are quite different from each other. $AlCl_3$ species promote the pathway that involves incorporation of furan rings (possibly HMF to 2,5-dioxo-6-hydroxyhexanal, or DHH), while $SnCl_4$ species promote probably the fragmentation of glucose and fructose prior to the formation of HMF. It is also unclear what fructose degradation intermediates participate in humins formation. Moreover, the amount of humins was estimated as the balance between the initial reactant and the known detectable products rather than being directly measured. Prior kinetics studies were carried out with stirring, while in our study the reactants were not stirred in order to avoid disturbance to the X-ray measurement. To investigate the effect stirring, the concentration profiles of reactants and products were compared at 80 ˚C with 10 wt% fructose as reactant and 1 mol/L HCl as catalyst with and without stirring. The conversion and yields, including that of humins, are similar when stirring was used (Figures S3a and S3c) as compared to without stirring (Figures S3b and S3d). In summary, both model assumptions and transport effects may have led to the observed differences in the humins formation rates starting from fructose as the substrate.

To investigate the effect of substrate, a solution containing 10 wt% HMF and 1 mol/L HCl (pH=0) and another containing 10 wt% fructose and 1 mol/L HCl (pH=0) were heated at 70 ºC. With HMF as the substrate, large precipitates formed quickly and the R_g exceeded the instrument limit at 80 ºC, which was the lowest temperature used in the fructose experiments. To overcome this problem, a lower temperature of 70 ºC was used and data was collected at longer reaction times compared to those shown in Figure 5. Representative scattering patterns in Figure 6a show that the scattered intensity of HMF-derived humins at low q values (0.0001 $Å^{-1}$) is approximately 10 times greater than that of fructose-derived humins. As was the case with fructose, no useful information could be extracted from the high q regime (>0.01 $Å^{-1}$) data, suggesting lack of structural features in sizes smaller than 200 Å. Therefore, no useful information can be extracted from the high q data for fructose. By extrapolation of the Arrhenius plot shown in Figure 3, we estimate a growth rate of fructose-derived humins at 70 ºC to be 2.32 nm/min, which is slightly higher than the growth rate of 2.03±0.04 nm/min for HMF-derived humins (Figure 6b). The comparable growth rate may indicate a common intermediate for growth, irrespective of the substrate (fructose vs. HMF) and similar particle volumes, assuming a similar growth mechanism. Given the dependence of growth rate on HMF concentration (see below), and the fact HMF concentration in fructose experiments increases with time at short times, it is difficult to perform further quantitative comparison of the substrates. Development of a model that estimates the HMF concentration and humins formed in fructose experiments and subtracts the humins produced in direct HMF experiments from those formed in fructose experiments will be needed to compare the relative contributions of substrates to humins. Therefore, the significantly higher I(q) of HMF-derived humins at low values of q can be attributed to a greater number of

humins particles formed. This is consistent with the conclusions of Lund and coworkers[17] and suggests that the direct formation of humins from fructose is slower. Instead, the predominant mechanism of humins formation is condensation of HMF molecules or its derivatives. Since the HMF concentration during the fructose reaction is low (Figures S3a, S4a, S5a, and S6a), the humins formation pathway involving the coupled condensation between fructose and HMF molecules could not be assessed from our data.

In the HMF experiments, the number of particles per volume increases over time (Figure 6c), similarly to what is seen at higher fructose concentration experiments but opposite from the behavior at low fructose concentrations (Figure 5c). The change in the number of particles at reaction times longer than 500 min could not be observed due to the rapid increase of the volume fraction leading to multiple scattering and particle-to-particle interactions under which the model assumptions about the structure factor no longer hold.

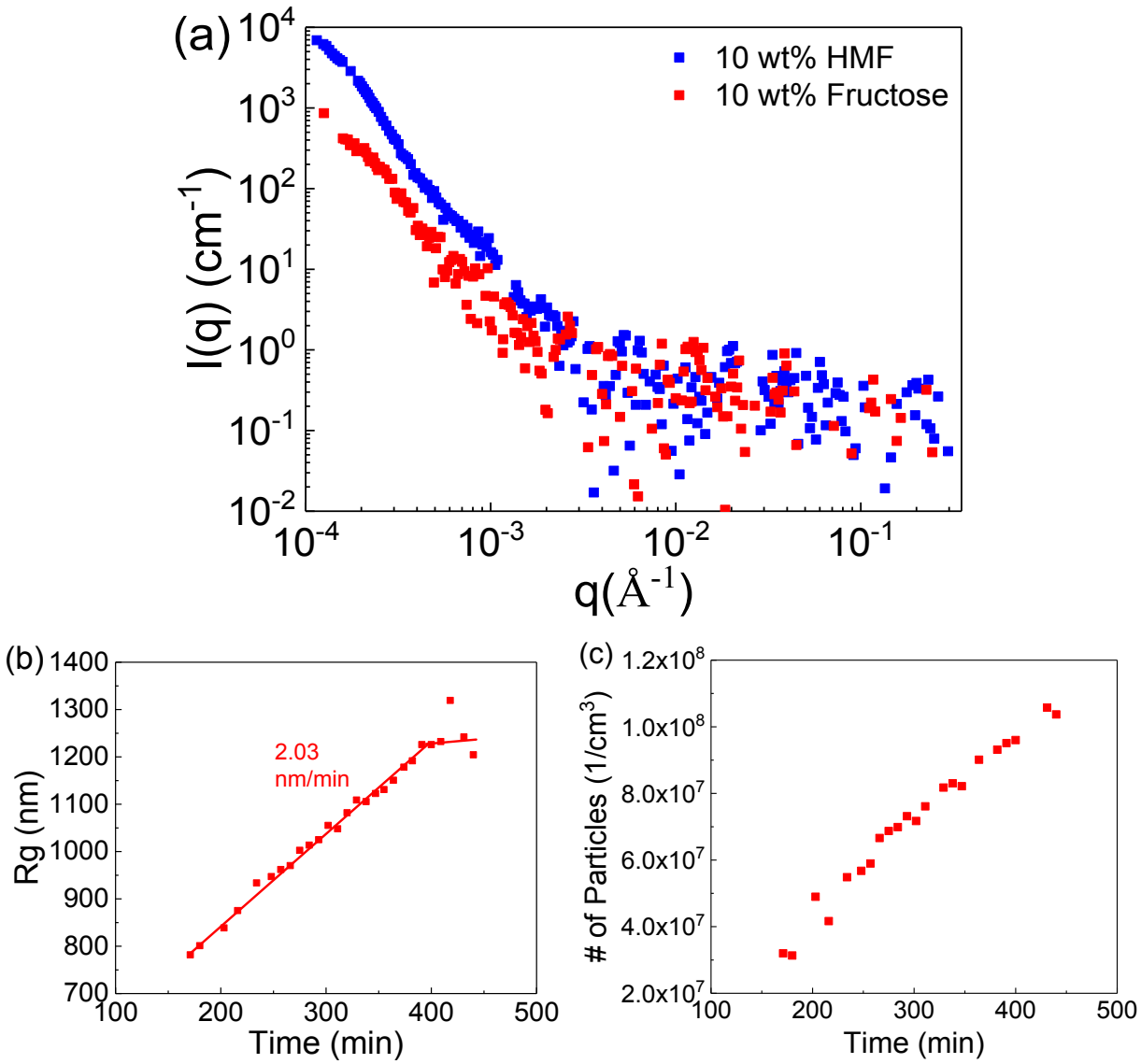

Figure 6. (a) Scattered intensities of humins originating from 10 wt% fructose and 10 wt% HMF solutions heated at 70 °C and pH of 0, taken at 449 min of reaction time. (b) and (c) Evolution of the corresponding R_g and number of particles as a function of time for the HMF solution. The growth rate value indicated corresponds to the growth (initial) regime.

We also varied the initial concentration of HMF between 2.5 and 10 wt% and estimated the rate of particle growth. The effect of initial HMF concentration was not studied in our prior work.[6] The growth rate increases with the initial HMF concentration, as shown in Figure 7. A second-order polynomial fit was used. A log-log plot shown in Figure 7b gave a slope between 1 and 2, as well as a low coefficient of determination (R^2). The nonlinear dependence of the growth rate of humins on HMF concentration underscores the complexity of the growth pathways of humins. We attribute this nonlinearity to the multiple paths contributing to growth, including condensation between HMF molecules, the condensation of HMF with water-soluble humins oligomers, and the addition of HMF to the surface of humins particles. In Figure 5, the growth rate barely changed when the initial fructose concentration was increased five-fold, from 10 wt% to 50 wt%. This zero-order dependence of growth rate on the fructose substrate concentration is in sharp contrast to the strong dependence of growth rate on the HMF substrate concentration. Taking Figures 5-7 together further underscores the limited effect fructose plays on the growth of humins compared to the dominant role of HMF.

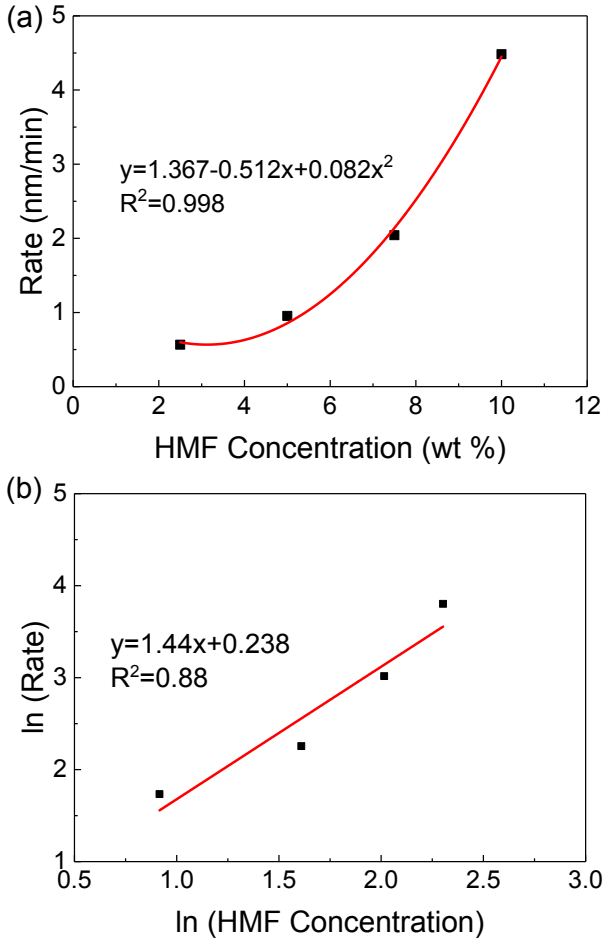

Figure 7. (a) Humins growth rate at different initial HMF concentrations of 2.5 wt%, 5 wt%, 7.5 wt% and 10 wt%. A second-order polynomial fit is shown here. (b) Log-log plot for humins formation rate vs. initial HMF concentration. Reactions at: 80 °C and pH=0.

Overall, the results can be rationalized by considering the HMF concentration as key in condensation chemistry for inception of new particles and growth of existing ones and the competing mechanisms controlling population size and growth rate. Specifically, the change in particle population is dictated by (1) the inception of new particles via condensation chemistry, controlled mainly from the level of HMF concentration and happening continuously as the increasing polydispersity indicates (Figure 4), and (2) particle agglomeration and precipitation of larger, denser, or less soluble particles that reduce the number of particles. R_g increases due to monomer condensation and particle aggregation and decreases when particles crash out of solution. Due to difference in molecular weight, the HMF experiments have a higher initial molar concentration of substrate compared to fructose. Furthermore, the HMF concentration is low in low fructose concentration solutions (Figures S3-S6) and much lower than that when HMF is the substrate (Figure S7). Higher concentrations of fructose result in higher HMF concentrations. When the monomer condensation dominates due to a high HMF concentration, the population increases with time irrespective of the substrate; conversely, when the HMF concentration is low, the number of particles decreases with time after a fast, initial growth due to aggregation and/or precipitation dominating over condensation.

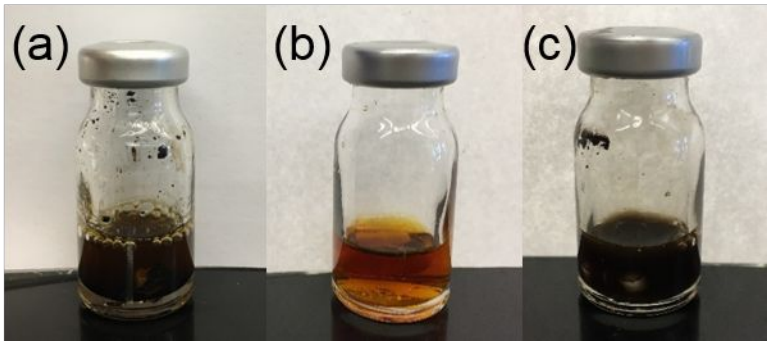

Figure 8 (a). Reaction mixture at 100% HMF conversion after heating at 120 °C for 48 h, before filtration and (b) after filtration using a 0.2 μm syringe filter. This long time results in complete HMF conversion. (c) After filtration, the solution was heated at 120 °C for another 24 h. Large humins particles still form even after all the HMF has been consumed.

To confirm the proposed pathway of oligomer aggregation by Tsilomelekis et al.,[6] we ran the reaction in HMF at 120 °C for 48 hours until 100% HMF conversion. A black solid suspension was formed at the end of the reaction (Figure 8a). The absence of HMF in the reaction mixture was confirmed by HPLC analysis, and FA and LA were the only soluble products detected in 11.1% and 62.1% carbon yields, respectively. The corresponding carbon yield of humins is 26.8%. Then a 0.20 μm pore size filter was used to remove the black solid precipitates. The filtrate is shown in Figure 8b. The filtrate containing FA, LA, and humins oligomers smaller than the filter pores was loaded into a clean vial and heated at 120°C for another 24 hours. After that,

the color of the suspension became darker, indicating the formation of visible, larger polymers, as shown in Figure 7c. This observation is consistent with a condensation polymerization growth model, as oligomers retain reactivity.

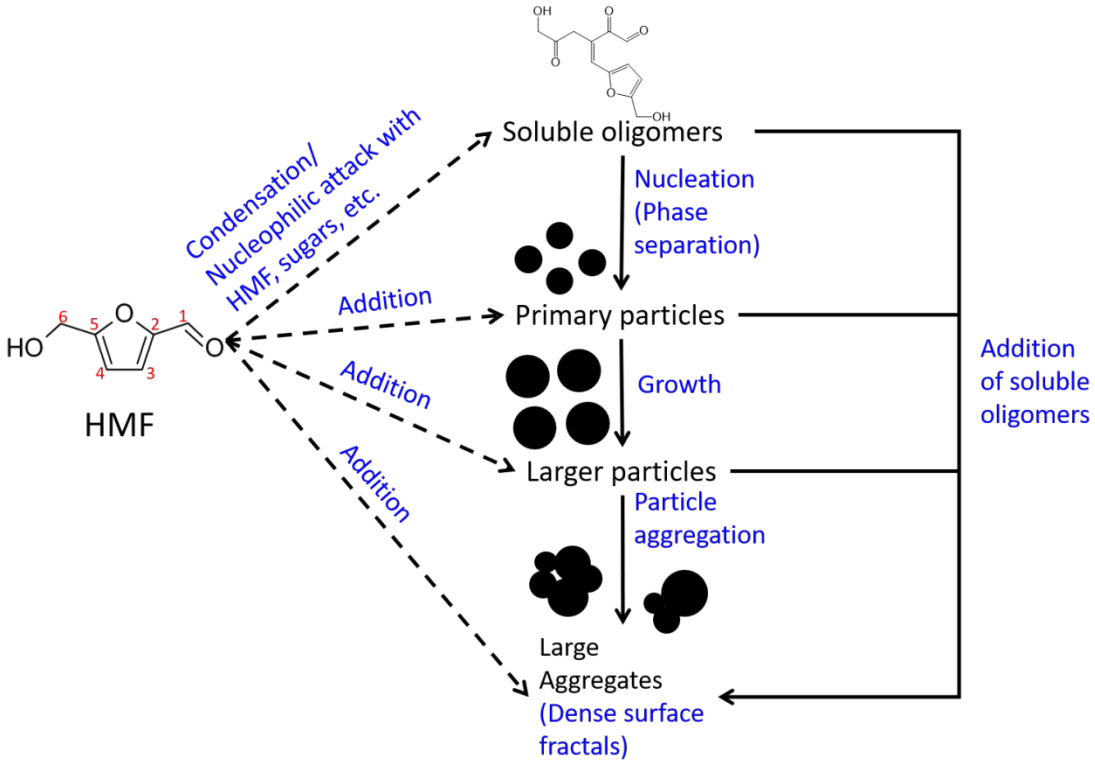

Scheme 1. Refined humins formation and growth network. Black dashed lines show the addition of HMF to other HMF molecules, soluble oligomers, primary particles, or particle aggregates. Black solid lines show the process of particle formation, growth and aggregation. The sizes of the black spheres are not drawn to scale and are for illustration purposes only.

Based on the above observations, we refine the network proposed by Tsilomelekis et al.[6] As shown in earlier work by Lund et al. and van Zandvoort et al., HMF undergoes ring opening, condensation[25] and nucleophilic attack[26] to form soluble oligomers. As the oligomers increase in size by addition of more HMF, a solubility threshold is reached leading to formation of primarily particles. The mechanism shown in Scheme 1 involves oligomers and small primary particles <20 nm. These primary particles, referred to above as a secondary population, are smaller than 20 nm and cannot be quantified by USAXS. The oligomers having degrees of polymerization between 3-10 have been identified in slow HMF degradation experiments at room temperature reported by Galkin et al.[27] Lund and coworkers also proposed energetically feasible structures of HMF dimers in their computational work.[25] However, it is quite possible that there is a continuum of sizes <20 nm. The primarily particles then grow into "larger particles" by addition of HMF units, soluble oligomers, or aggregation with other particles. At short times, the number of particles and polydispersity increase indicating that condensation chemistry to oligomers and aggregation to small primary particles dominate over particle growth leading to larger particles.

As the HMF concentration decreases and that of the particles increases, the aggregation between particles becomes eventually dominant and continues even after all the HMF has been consumed.

Next, we compare the formation of growth of humins with the well-studied silica particles. Although the formation and growth of humins have not been studied as much, the nucleation and growth of particles in general have been extensively studied using silica precipitated from aqueous solutions as the model system.[28-31] Here, a base catalyst, usually ammonia, is added to a tetraalkoxysilane in an alcohol solution. The reaction is described by the following equations:

$$\equiv SiOR + H_2O \xrightarrow{OH^-} \equiv SiOH + ROH \text{ (Hydrolysis)}$$

$$2 \equiv SiOH \xrightarrow{OH^-} \equiv SiOSi \equiv + H_2O \text{ (Condensation)}$$

Solid particles increase in size by molecular addition where soluble species deposit on the solid surface or by aggregation with other solid particles.[30] Herein, two extreme cases have been proposed for the growth of silica particles. Matsoukas et al. [31] presented a monomer addition model where the particle nucleation is the result of reaction between two hydrolyzed monomers. The hydrolysis step was found to be rate-limiting. Nucleation happened only in the earliest stage, and growth by monomer addition became dominant and the number of particles stayed constant thereafter. In this addition mechanism, the particle size distribution remains very narrow during growth until the end of the process. [32] Bogush et al. [30] presented an aggregative growth model where particles grow solely by aggregation with other particles. Small nuclei form throughout the entire reaction. Once the aggregates reach a certain size (and thereby a certain colloidal stability because of their surface charge), the growth continues only by aggregation with the small sub-particles and not by collisions with other (larger) particles.[33] Subsequently, the size distribution of the particles was rather uniform. The final equilibrium distribution and the size are determined by parameters such as the surface charge.[32]

Our results clearly indicate that despite silica and humins growth sharing reactive events rather than a classical nucleation mechanism, the signatures of growth are definitely different between the two systems.

Conclusions

We have used *in-situ* USAXS for the first time to investigate the evolution of size and morphology of growing humins particles from fructose and HMF. We show that the humins form fractal particles that grow at rates of 5-25 nm/min, depending on the reaction temperature. We estimated the apparent activation energy of humins growth from fructose to be 102±0.4 kJ/mol. Based on the nearly equal growth rates of fructose- and HMF-derived humins, combined with the larger particle population of HMF-derived humins, we find that condensation of HMF is the predominant mechanism for humins formation and fructose may simply physisorb onto humins.

For the first time, the inception and growth of humins from HMF have been connected to existing theories developed about the nucleation and growth of silica particles. The rate of humins growth was shown to be quadratic (or a power law of ~1.5) in initial HMF concentration, underscoring the complexity of humins growth pathways. Using USAXS, we were able to demonstrate the competition of humins inception and growth. When the HMF concentration is high, inception and growth by condensation chemistry dominate, the number of particles keeps growing, and the average radius of gyration keeps increasing. In contrast, when the HMF concentration is low, aggregation and precipitation dominate over condensation chemistry and the population decreases giving rise to a constant growth rate.

Acknowledgements

This work was financially supported by the Catalysis Center for Energy Innovation, an Energy Frontier Research Center funded by the U.S. Department of Energy, Office of Science, office of Basic Energy Sciences under Award Number DE-SC0001004. This research used resources of the Advanced Photon Source, a U.S. Department of Energy (DOE) Office of Science User Facility operated for the DOE Office of Science by Argonne National Laboratory under Contract No. DE-AC02-06CH11357. The authors would like to thank Dr. Ivan Kuzmenko, Dr. Ross Andrews, Dr. Jan Ilavsky, and Jiayi Fu for their help with operating the USAXS instrument, running experiments and fitting the data.

References

1. I. van Zandvoort, E. J. Koers, M. Weingarth, P. C. Bruijnincx, M. Baldus and B. M. Weckhuysen, *Green Chemistry*, 2015, **17**, 4383-4392.
2. J. J. Bozell, L. Moens, D. Elliott, Y. Wang, G. Neuenscwander, S. Fitzpatrick, R. Bilski and J. Jarnefeld, *Resources, conservation and recycling*, 2000, **28**, 227-239.
3. T. Hoang, E. Van Eck, W. Bula, J. Gardeniers, L. Lefferts and K. Seshan, *Green chemistry*, 2015, **17**, 959-972.
4. T. M. C. Hoang, L. Lefferts and K. Seshan, *ChemSusChem*, 2013, **6**, 1651-1658.
5. C. Rasrendra, M. Windt, Y. Wang, S. Adisasmito, I. Makertihartha, E. van Eck, D. Meier and H. Heeres, *Journal of Analytical and Applied Pyrolysis*, 2013, **104**, 299-307.
6. G. Tsilomelekis, M. J. Orella, Z. Lin, Z. Cheng, W. Zheng, V. Nikolakis and D. G. Vlachos, *Green Chemistry*, 2016, **18**, 1983-1993.
7. S. Constant, C. S. Lancefield, B. M. Weckhuysen and P. C. Bruijnincx, *ACS Sustainable Chemistry & Engineering*, 2016.
8. S. K. Patil and C. R. Lund, *Energy & Fuels*, 2011, **25**, 4745-4755.
9. J. Ilavsky, P. R. Jemian, A. J. Allen, F. Zhang, L. E. Levine and G. G. Long, *Journal of Applied Crystallography*, 2009, **42**, 469-479.
10. D. S. Sivia, *Elementary scattering theory: for X-ray and neutron users*, Oxford University Press, 2011.
11. B. Hammouda, *NIST Center for Neutron Research, Gaithersburg, MD, USA. http://www. ncnr. nist. gov/staff/hammouda/the_SANS_toolbox. pdf*, 2008.
12. J. Ilavsky and P. R. Jemian, *Journal of Applied Crystallography*, 2009, **42**, 347-353.

13. B. Hammouda, Probing Nanoscale Structures-the SANS Toolbox, https://www.ncnr.nist.gov/staff/hammouda/the_SANS_toolbox.pdf, (accessed March 4th, 2017).
14. B. Kuster and H. Der Van Steen, *Starch-Stärke*, 1977, **29**, 99-103.
15. B. Girisuta, L. Janssen and H. Heeres, *Green Chemistry*, 2006, **8**, 701-709.
16. W. H. Carothers, *Transactions of the Faraday Society*, 1936, **32**, 39-49.
17. S. K. Patil, J. Heltzel and C. R. Lund, *Energy & Fuels*, 2012, **26**, 5281-5293.
18. B. F. Kuster and H. M. Temmink, *Carbohydrate research*, 1977, **54**, 185-191.
19. B. F. Kuster and H. S. van der Baan, *Carbohydrate research*, 1977, **54**, 165-176.
20. T. D. Swift, C. Bagia, V. Choudhary, G. Peklaris, V. Nikolakis and D. G. Vlachos, *ACS Catalysis*, 2013, **4**, 259-267.
21. H. Kimura, M. Nakahara and N. Matubayasi, *The Journal of Physical Chemistry A*, 2013, **117**, 2102-2113.
22. T. D. Swift, H. Nguyen, A. Anderko, V. Nikolakis and D. G. Vlachos, *Green Chemistry*, 2015, **17**, 4725-4735.
23. K. R. Enslow and A. T. Bell, *ChemCatChem*, 2015, **7**, 479-489.
24. P. Ramesh, A. Kritikos and G. Tsilomelekis, *Reaction Chemistry & Engineering*, 2019, **4**, 273-277.
25. J. Heltzel, S. K. Patil and C. R. Lund, in *Reaction Pathways and Mechanisms in Thermocatalytic Biomass Conversion II*, Springer, 2016, pp. 105-118.
26. I. van Zandvoort, Y. Wang, C. B. Rasrendra, E. R. van Eck, P. C. Bruijnincx, H. J. Heeres and B. M. Weckhuysen, *ChemSusChem*, 2013, **6**, 1745-1758.
27. K. I. Galkin, E. A. Krivodaeva, L. V. Romashov, S. S. Zalesskiy, V. V. Kachala, J. V. Burykina and V. P. Ananikov, *Angewandte Chemie International Edition*, 2016, **55**, 8338-8342.
28. H. Boukari, J. S. Lin and M. T. Harris, *Journal of Colloid and Interface Science*, 1997, **194**, 311-318.
29. D. L. Green, J. S. Lin, Y. F. Lam, M. Z. C. Hu, D. W. Schaefer and M. T. Harris, *Journal of Colloid and Interface Science*, 2003, **266**, 346-358.
30. G. H. Bogush and C. F. Zukoski, *Journal of Colloid and Interface Science*, 1991, **142**, 19-34.
31. T. Matsoukas and E. Gulari, *Journal of Colloid and Interface Science*, 1989, **132**, 13-21.
32. H. Boukari, J. S. Lin and M. T. Harris, *Chemistry of Materials*, 1997, **9**, 2376-2384.
33. A. Van Blaaderen, J. Van Geest and A. Vrij, *Journal of colloid and interface science*, 1992, **154**, 481-501.